THE ASTROPHYSICAL JOURNAL, 374:72–82, 1991 June 10

NEW OBSERVATIONS OF THE GAS CLOUD ASSOCIATED WITH THE QUASAR-GALAXY PAIR 3C 232/NGC 3067

JOHN T. STOCKE,[1] JAMES CASE,[2] MEGAN DONAHUE,[1,3] J. MICHAEL SHULL,[4] AND THEODORE P. SNOW
Center for Astrophysics and Space Astronomy, Department of Astrophysical, Planetary, and Atmospheric Sciences, University of Colorado, Campus Box 391, Boulder, CO 80309
Received 1990 June 18; accepted 1990 November 28

ABSTRACT

We present new optical Na I and Ca II spectra, new Hα images, and archival *IUE* ultraviolet spectra of the quasar-galaxy pair 3C 232/NGC 3067, to study the H I gas cloud seen in 21 cm emission between the eastern edge of NGC 3067 and 3C 232. High-resolution optical spectra show two, and possibly three, absorption systems in Ca II and Na I, with a large velocity spread ($\Delta v \approx 160$ km s^{-1}); *IUE* spectra show Fe II and Mg II absorption. The strongest system is coincident with narrow 21 cm absorption at $cz = 1420$ km s^{-1} and has Na I/Ca II ≈ 0.7–2, suggesting that the Ca-bearing grains have not been strongly disturbed. The H I absorption is most likely produced by cold ($T \leq 300$ K) gas comprising 1%–2% of the 3×10^{21} cm^{-2} of warm H I ($T \approx 8000$ K) seen in 21 cm emission. At a distance of (14.7 Mpc)h^{-1}, this cloud has mass $\sim(10^8\ M_\odot)h^{-2}$, linear extent $\sim$(2.5 kpc)h^{-1}, and mean hydrogen density $n_{\rm H} = (0.42\ {\rm cm}^{-3})h$.

We detect no Hα, to a limit of 27.5 mag arcsec^{-2}, coincident with the H I cloud in broad-band *R* images or in narrow-band redshifted CCD images. The absence of Hα sets a limit of $\Phi_{\rm ion} < 8.35 \times 10^4$ photons s^{-1} on the ionizing photon flux, corresponding to $I_0 \equiv I_\nu(13.6\ {\rm eV}) < 1.8 \times 10^{-22}$ ergs cm^{-2} s^{-1} Hz^{-1} sr^{-1} on the diffuse extragalactic ionizing flux. The ionization balance of Na I and Ca II can provide even lower limits, $I_0 \approx [(1\text{–}6) \times 10^{-23}$ ergs cm^{-2} s^{-1} Hz^{-1} sr$^{-1}]h$, assuming depletion factors $d_{\rm Na} = 0.25$ and $d_{\rm Ca} = 0.1$ for Na and Ca. From the flux of ionizing photons inferred from *IUE* spectra of 3C 232, the Hα limit implies that the quasar must lie at least (25 kpc)h^{-1} behind the H I cloud, and the Na-Ca limits imply a distance of at least (25–66 kpc)$h^{-3/2}$. While this does not rule out the noncosmological redshift interpretation for the quasar, 3C 232 is unlikely to be the perturber that stripped the H I finger from NGC 3067. The H I is most likely a chance projection at the quasar position and offers no additional support for the association of the pair.

Subject headings: galaxies: individual (NGC 3067) — galaxies: interactions — interstellar: matter — quasars — ultraviolet: spectra

1. INTRODUCTION

Projected pairs of quasars and galaxies have played an important role in the historical debate over the cosmological nature of the redshift. Depending on the interpretation of this redshift, one may also use these pairs to search for tidal perturbations, gravitational lensing by halo stars, and absorption by gas in the halo of the intervening galaxy. In this paper we discuss new absorption and emission results on the quasar-galaxy pair 3C 232/NGC 3067, and we use them to constrain parameters of the associated gas cloud. Limits on the ionizing flux incident on this cloud also provide constraints on the location of the quasar 3C 232 and on the extragalactic ionizing flux.

Attention was first drawn by Burbidge et al. (1971) to the projection of the quasar 3C 232 and the nearby bright Sb III spiral galaxy NGC 3067. This galaxy-quasar pair was one of four that constituted statistical evidence for an overabundance of 3C quasars near bright galaxies. This quasar is also one of the brightest of five known quasars whose spectra exhibit absorption lines due to a nearby galaxy (Haschick & Burke 1975; Boksenberg & Sargent 1978; Boksenberg et al. 1980; Blades, Hunstead, & Murdoch 1981; Burbidge et al. 1988).

The quasar 3C 232 appears on the sky $\sim 2'$ (113″.5) above the center of the visible disk of NGC 3067 (Rubin, Thonnard, & Ford 1982, hereafter RTF). For a Hubble constant $H_0 = (100$ km s^{-1} Mpc$^{-1})h$, this angular separation corresponds to a projected distance of (8.1 kpc)h^{-1} at an assumed distance of (14.7 Mpc)h^{-1} to NGC 3067. In the radio spectrum of 3C 232 (redshift $z_e = 0.533$) Haschick & Burke (1975) detected narrow ($\Delta v < 5.5$ km s^{-1}) absorption due to H I at the redshift (1418 ± 2 km s^{-1}) of the foreground galaxy NGC 3067. This discovery was confirmed by Grewing & Mebold (1975), and the detection was followed by higher resolution H I observations (Wolfe 1979; RTF) that found a heliocentric redshift $cz_a = 1420 \pm 0.5$ km s^{-1} and a full width at half-maximum (FWHM) of the 21 cm absorption between 3.6 and 3.7 km s^{-1}. The inferred H I column density for the absorption system is (5.8×10^{19} cm^{-2})(T_s/300 K), where we have assumed a spin temperature $T_s = 300$ K corresponding to the observed 3.7 km s^{-1} line width. We have also corrected an apparent factor of 2 error in the integrated 21 cm line optical depth tabulated by RTF (0.106 rather than 0.211 km s^{-1}).

In high-dispersion optical spectra Boksenberg & Sargent (1978, hereafter BS) found Ca II K and H absorption at the same redshift as the H I (mean velocity 1406 ± 11 km s^{-1}) with observed-frame equivalent widths of 430 ± 40 mÅ (K) and 260 ± 40 mÅ (H). The Ca II lines were noticeably broader (FWHM 90 ± 15 km s^{-1}) than the spectral resolution (50–60

[1] Visiting Astronomer, National Optical Astronomy Observatories, Tucson, AZ.

[2] Postal address: University of Massachusetts, Department of Physics and Astronomy, Amherst, MA 01002.

[3] Postal address: The Observatories of the Carnegie Institution of Washington, 813 Santa Barbara Street, Pasadena, CA 91101.

[4] Also Joint Institute for Laboratory Astrophysics, University of Colorado and National Institute of Standards and Technology.

km s^{-1}), and Ca II K seemed to possess a red wing (see Fig. 2 in BS). They did not detect the Na I D lines on a single attempt at low signal-to-noise ratio, and thus placed modest limits of 250 mÅ on the Na I equivalent widths. They also argued that the Ca II lines were likely to possess two or more unresolved velocity components.

More recently, low-dispersion (7 Å) ultraviolet observations (Bergeron, Savage, & Green 1987) of 3C 232 made with the *International Ultraviolet Explorer* (*IUE*) satellite provided a detection of this absorption system in Mg II and set limits on the presence of C IV and Si IV. In a paper devoted to the ultraviolet variability of 3C 232, Bruhweiler, Kafatos, & Sofia (1986) mentioned the presence of Mg II absorption near 2800 Å but attributed it to gas in the Milky Way halo.

Because 3C 232 appears so far above the visible disk of NGC 3067 on the sky, there has been a continuing debate (RTF; BS) over whether these absorption lines arise in the extended disk or in the halo of the spiral galaxy. The spiral is viewed nearly edge-on ($i = 68^{+4}_{-3}$ degrees; RTF), so that the line of sight to 3C 232 intercepts the disk plane at several Holmberg radii, $r = (22^{+4}_{-3}$ kpc)h^{-1}. The Arecibo observations (Wolfe 1979; RTF) showed that no large H I structure exists beyond the visible disk of NGC 3067, and RTF concluded that the absorption arises in a disk significantly warped toward 3C 232 on the sky. On the other hand, if the absorptions arise from cool halo gas, the halo must be enormous. Therefore, the morphology of the absorbing gas has important implications for the total masses of galaxies and for the observed frequency of high-redshift absorption systems toward quasars.

A recent VLA map of this system (Carilli, van Gorkom, & Stocke 1989, hereafter CvGS) in the 21 cm line of H I resolved the controversy by detecting a narrow "finger" of H I emission extending from the western edge of NGC 3067 across the position of 3C 232 on the sky. A truncation in the H I contours at the west edge of the disk of NGC 3067 suggests that the absorption cloud toward 3C 232 arises from material pulled out of the disk rather than from a large gaseous halo. The H I finger may have been produced by a tidal interaction between NGC 3067 and a small companion galaxy, but at present no likely companion galaxy has been found within (0.5 Mpc)h^{-1}. A possible H I cloud north-northeast of 3C 232 was seen with M(H I) $\approx (10^8\ M_\odot)h^{-2}$, which could be a gas-rich dwarf galaxy. However, the reality of this northern H I "cloud" is suspect, since it lies at the position of a side lobe of the continuum source in 3C 232. Further careful mapping at 21 cm is needed to confirm the northern cloud.

In this paper we report new observations of the absorption system in 3C 232 due to NGC 3067. In § 2 we describe high-resolution optical spectra of this absorption system at Ca II H and K and at Na I D1 and D2, in which the absorption observed by BS is resolved into two and possibly three components at significantly different velocities. The velocity spread of these components ($\Delta v \approx 160$ km s^{-1}) is similar to that seen in C IV toward the Large Magellanic Cloud (York et al. 1986) and toward quasars at higher redshift. In § 3 we present an analysis of the available *IUE* low-dispersion spectra of 3C 232, in which we detect Mg II and Fe II absorption lines and place upper limits on C IV, Si IV, Si II, and Lyα absorption. The *IUE* spectra also allow us to extrapolate the energy distribution of 3C 232 to the Lyman limit and thereby obtain an estimate of the quasar's ionizing flux. In § 4 we present new deep imaging in the red continuum and redshifted Hα emission line. In § 5 we use details of the H I, Na I, and Ca II absorption and the Hα imaging to set limits on the ionizing flux incident on the H I finger and absorbing cloud. The Na and Ca limits, together with the quasar ionizing flux estimated from *IUE*, suggest that 3C 232 is at least (25–66 kpc)$h^{-3/2}$ away from the cloud, independent of assumptions about the nature of the quasar's redshift but depending on the assumed distance of (14.7 Mpc)h^{-1} to the galaxy NGC 3067, based on its observed redshift.

2. SPECTROSCOPY

In high-resolution optical spectra of 3C 232 we detected Na I and Ca II absorption lines with two or three velocity components around velocity $cz \approx 1420$ km s^{-1}. The strongest of these components agrees with the velocity of the narrow 21 cm absorption line, and we believe it to dominate the column density. In this section we describe the results of an analysis of archival *IUE* (SWP and LWP/LWR) low-resolution spectra that detect Fe II and Mg II absorption lines. Table 1 provides a journal of the optical and ultraviolet observations used in this paper.

TABLE 1

3C 232: Journal of Observations

Date	Wavelength Region (Å)	Aperture Size	Instrumental FWHM (Å)	Integration Time (minutes)	Limiting W_λ (mÅ)
		Optical			
1983 Nov 29	5875–5949	1".0	0.2	69	15
1984 Feb 2	5888–5952	1.0	0.2	75	15
1984 Feb 2	5873–5947	1.0	0.2	140	15
1984 Nov 23	3900–4020	2.5	0.6	190	50
1987 Mar 28	3650–4650	2.5	1.1	80	95
		Ultraviolet (*IUE*)			
1978 Oct 30	LWR 2752	10" × 20"	5–7	435	500
1979 Jun 4	LWP 4680	...	...	230	500
1979 Nov 28	LWP 6242	...	...	385	500
1985 Mar 20	LWR 17661	...	...	400	500
1979 May 8	SWP 5169	...	...	865	500
1980 Apr 25	SWP 8825	...	...	395	500
1985 Mar 21	SWP 25496	...	...	420	500

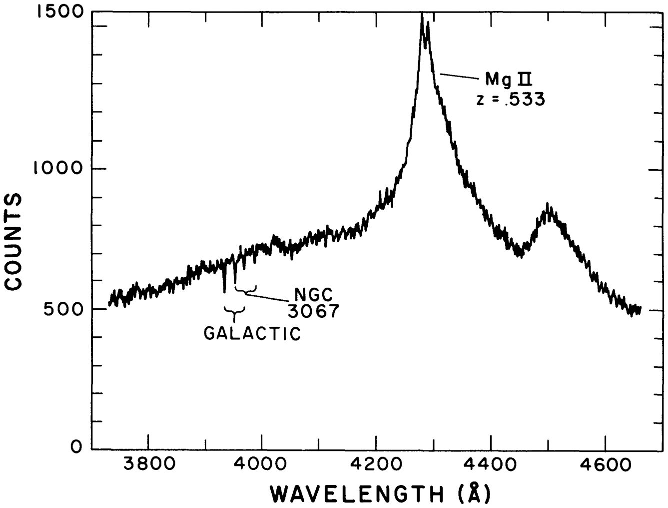

FIG. 1.—Spectrum of 3C 232 with 1 Å resolution, obtained with the MMT blue spectrograph using the 832 line mm^{-1} grating in second order. The locations of the Ca II K and H absorption lines due to NGC 3067 are well away from any sharp emission features.

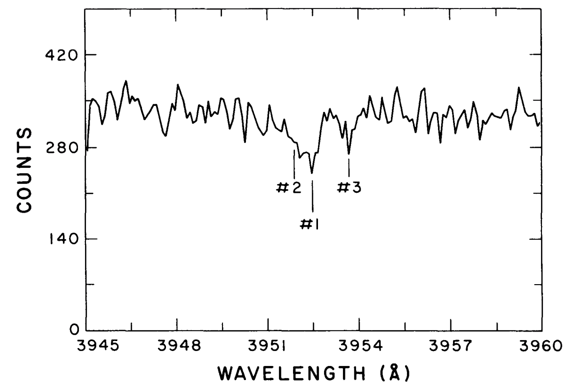

FIG. 2*a*

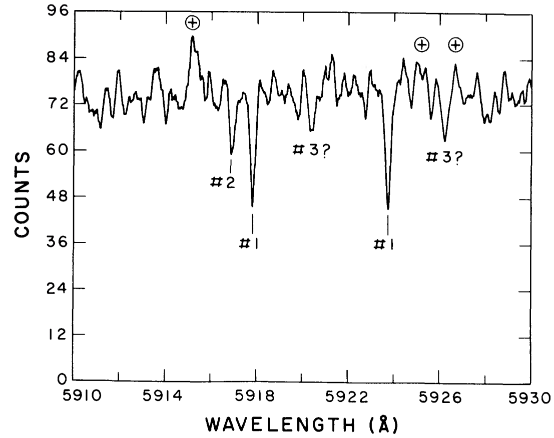

FIG. 2*b*

FIG. 2.—(*a*) MMT blue spectrograph and "echellette" grating spectrum (40 km s^{-1} resolution) of 3C 232 in the vicinity of the Ca II K line showing the three proposed velocity systems due to absorbing gas associated with NGC 3067. The velocity of system 1 is constant with the H I 21 cm detection of Haschick & Burke (1975). Wavelengths are given in observed frame. (*b*) MMT echelle spectrum of 3C 232 at Na I D. This 12 km s^{-1} resolution spectrogram detects two of the three proposed velocity systems; positions for the third, not clearly detected, system are shown. Earth symbols indicate expected positions of airglow emission lines of OH in this spectrum without sky subtraction. Wavelengths are given in observed frame.

2.1. *Optical Absorption Lines*

Optical observations of the Ca II H and K lines and the Na I D lines in the 3C 232/NGC 3067 system were made with the Multiple Mirror Telescope (MMT)[5] spectrograph and echelle spectrograph and are shown in Figures 1–3. Table 2 summarizes the results. Figure 1 is a low-resolution blue spectrum of 3C 232 showing the location of the Ca II absorption lines due to both NGC 3067 and the Milky Way. These lines are well away from any emission lines due to the quasar itself or from strong telluric lines. Besides the four Ca II absorption lines, our two blue spectrograms detected no other lines in common with BS; in particular, we do not confirm the absorption system at $z_a = 0.5132$ proposed by BS. The broad emission feature near 4500 Å is likely the Fe II λ2950 blend (Grandi 1981).

Our high-resolution observations used the MMT spectrograph plus "echellette" grating in 13th and 14th orders simultaneously (see Fig. 2*a*). Owing to the fortuitous positions of the Ca II lines in 3C 232 with respect to the blaze wavelengths of the echellete grating, it was possible to obtain simultaneous coverage of these lines in two adjacent orders through the same interference filter. The detector was a pair of cooled linear Reticon arrays behind a train of image intensifiers and a microchannel plate. We used an order-separating interference filter to isolate orders 13 and 14 of the spectrum. The resulting data have 40 km s^{-1} resolution and ~400 Å coverage in each order. The final spectrum is the result of a total of about 3 hours of integration and is sky-subtracted.

The echellette spectrum easily detected both Ca II H and K near the redshift of NGC 3067. Instead of the single broadened line seen by BS, our Ca II spectrum contains evidence for three separate velocity components. Figure 2*a* illustrates a summation of the two adjacent orders for Ca II K. The equivalent widths in Table 2 have been corrected for order overlap, small at the positions of the absorptions, and are consistent with the equivalent widths reported by BS. Our total observed-frame equivalent widths for Ca II are 390 ± 50 mÅ (K) and 220 ± 50 mÅ (H), compared with the 430 ± 40 mÅ (K) and 260 ± 40 mÅ (H) obtained by BS. Observed-frame values differ by only 1–2 mÅ from rest-frame values, since the redshift is low.

The MMT echelle spectrum of the Na I D lines (Fig. 2*b*) has an instrumental resolution of 12 km s^{-1} and a full wavelength coverage of 65 Å, corresponding to a single echelle order. At this resolution the brightness of the night sky is negligible, except at the wavelengths of airglow emission lines. In the Na I D region, telluric sodium partially obscures the Galactic D lines, but the vicinity of the 3C 232/NGC 3067 absorption system contains only some weak OH features (Hubbard et al. 1983) at positions marked on Figure 2*b*. A detector dark signal of 28 counts is the dominant source of additional light in the system and has been subtracted from the data in Figure 2*b*; the sky has not been subtracted. The total integration time on source was 284 minutes at two epochs and three central wavelengths, altered slightly between observations to shift the pixels

[5] Observations reported here used the Multiple Mirror Telescope Observatory, a joint facility of the Smithsonian Institution and the University of Arizona.

FIG. 4a

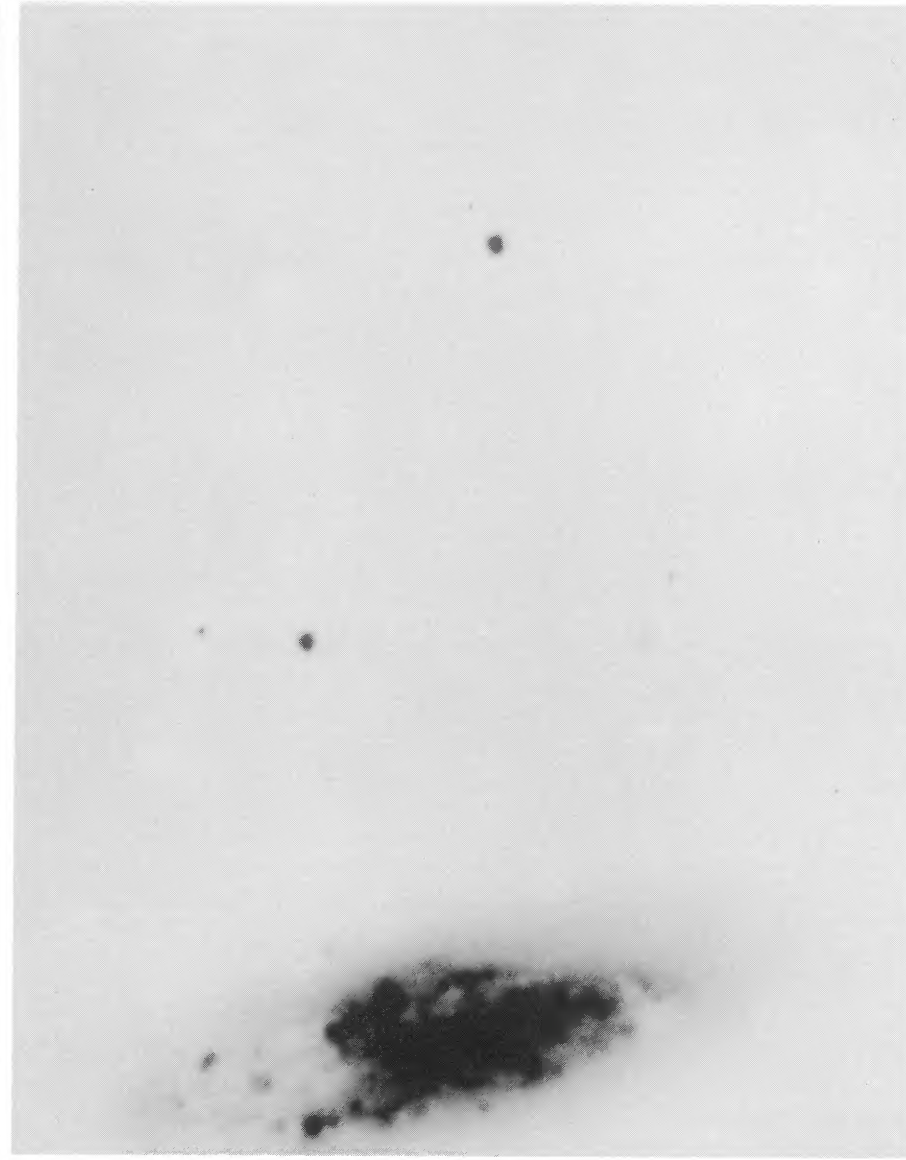

FIG. 4b

FIG. 4.—(*a*) Low-contrast optical image of the NGC 3067 and 3C 232 system in "pure Hα emission," minus the continuum, taken in a 40 minute exposure at the Kitt Peak 2.1 m telescope. The seeing is $\sim 0''.8$. (*b*) High-contrast image of the same Hα frame, showing the background level clearly. The bad CCD line above the disk was not used in the flux limits. (*c*) Ten minute frame taken with the Gunn *R* filter. (*d*) Contour map of H I overlaid on a broad-band blue image kindly provided by H. C. Arp. This image was previously published in CvGS and has a different field of view to include the possible northern cloud.

STOCKE et al. (see 374, 76)

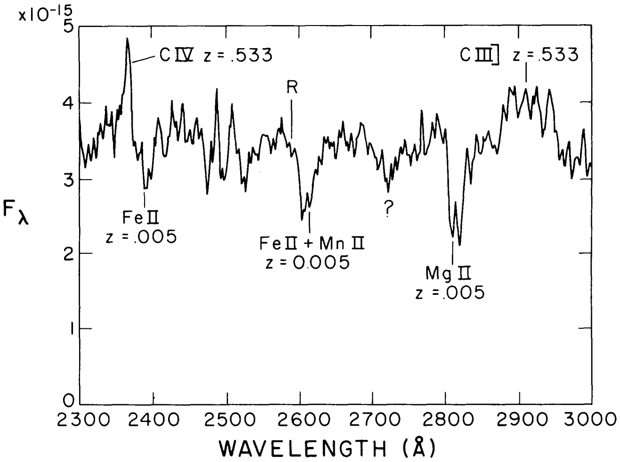

FIG. 3*a*

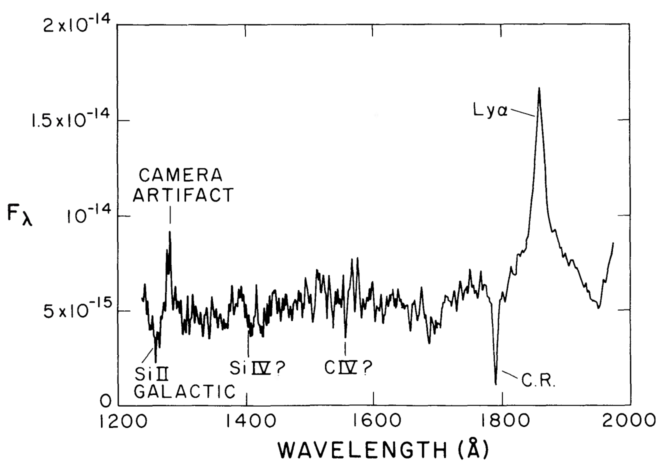

FIG. 3*b*

FIG. 3.—(*a*) Long-wavelength *IUE* camera co-addition of 1450 minutes of integration time on 3C 232, showing F_λ (ergs cm^{-2} s^{-1} Å^{-1}). Emission lines due to the quasar are indicated, as is a detector reseau. Absorption lines due to gas associated with NGC 3067 are also detected, although at this resolution the various velocity components are inseparable. (*b*) Short-wavelength *IUE* camera co-addition of 1690 minutes of integration time on 3C 232. Only upper limits are obtained for absorption lines due to NGC 3067 from these data. C.R. denotes a bright cosmic ray in the area of sky subtraction. The feature marked "camera artifact" was erroneously identified by Bruhweiler, Kafatos, & Sofia (1986) as blended emission lines of O II and O III (see text).

on the absorption lines and allow for independent confirmation.

At Na I we detected the strongest system (No. 1) in both D1 and D2 at a velocity consistent with the H I detections of Haschick & Burke (1975), Wolfe (1979), and RTF. The D1 and D2 lines are of comparable strength and clearly saturated. The D2 line has a 4 σ detection of a system (No. 2) at a lower velocity, although this system is not confirmed in the weaker D1 line. There is also marginal (2.5 σ) evidence for a third system (No. 3) at Ca II K. Because the position of the Na I D1 line is "sandwiched" between the two telluric emission features, we claim no detection of system 3 in Na I. The three Na I lines detected in the echelle data are all unresolved at 12 km s^{-1} resolution.

Each of the three proposed velocity systems is seen in two or more independent spectra. System 1 is definitely detected in Na I, Ca II, and H I (21 cm). The *IUE* spectra presented in § 3 provide detections of Mg II and Fe II, which must arise in all three systems ($\Delta v \approx 160$ km s^{-1}) in order to achieve the observed 5–6 Å equivalent widths. System 2 is detected at Na I D2 and is visible at Ca II K in the echellette data (Fig. 2*a*) as a blue wing on the system 1 line. System 3 is detected (2.5 σ) at Ca II K in our echellette data and as a red wing in the Ca II K data of BS. Owing to the nondetection of system 3 in our highest resolution data (Na I D spectra, Fig. 2), we quote in Table 2 the velocity of the Ca II K line from Figure 2. The other two system velocities are taken from the Na I MMT echelle data. All velocities quoted are heliocentric.

Other absorption lines suggested by BS are not seen in our data. For example, BS reported a second absorption system in 3C 232 at $z_a = 0.513$ based on detections of Fe II λ2586 at 3912.7 Å ($W_\lambda = 180 \pm 40$ mÅ), of Fe II λ2599 blended with Galactic Ca II K, and of Mg II K λ2795 at 4231 Å. In our MMT echellette spectrum, the only potential absorption line near the wavelength of redshifted Fe II λ2586 is a 2 σ feature at 3916.4 Å, too far from the feature reported by BS to be the same. A 3 σ upper limit of 50 mÅ can be placed on the presence of absorption at 3912.7 Å from our echellette data. The spectrum at 1 Å resolution (Fig. 1) also does not detect the suggested Mg II K line ($z = 0.513$) at a limiting (3 σ) equivalent width of 150 mÅ.

3. ULTRAVIOLET ABSORPTION LINES

We have analyzed archival ultraviolet spectra of 3C 232 taken at several epochs (Table 1) with the short- and long-

TABLE 2

ABSORPTION LINES IN 3C 232 DUE TO NGC 3067[a]

Line	System 1[b]	System 2[b]	System 3[b]	Total
Na I D2	101 ± 15 mÅ	63 ± 15 mÅ	15 ± 15 mÅ	179 ± 25 mÅ
Na I D1	121 ± 15 mÅ	≤ 15 mÅ	15 ± 15 mÅ	136 ± 20 mÅ
Ca II K	170 ± 50 mÅ	100 ± 50 mÅ	120 ± 50 mÅ	390 ± 60 mÅ
Ca II H	120 ± 50 mÅ	50 ± 50 mÅ	50 ± 50 mÅ	220 ± 50 mÅ
Mg II K	...	...	...	3.8 ± 0.7 Å
Mg II H	...	...	...	4.3 ± 0.7 Å
Fe II λ2599 and Mn II $\lambda\lambda$2576, 2594	...	...	...	5.7 ± 1.2 Å
Fe II λ2382	...	...	...	6.0 ± 2.5 Å
C IV λ1551	...	...	...	≤ 1.5 Å
Si IV λ1398	...	...	...	≤ 1.0 Å
Si II λ1206	...	...	...	≤ 1.5 Å

[a] Fe II λ2382 is uncertain because of C IV emission.

[b] The three components have velocities V(helio) = 1417 ± 2 km s^{-1} (system 1), 1369 ± 2 km s^{-1} (system 2), and 1530 ± 10 km s^{-1} (system 3).

wavelength cameras (SWP, LWP, and LWR) aboard *IUE*. Table 2 and Figure 3 show the results. The spectra have been obtained by reextracting, shifting, and co-adding the individual *IUE* archive spectra using the Gaussian extraction (GEX) program developed for faint-source spectra (Urry & Reichert 1987). Our procedure cross-correlates individual spectra to align individual wavelength vectors properly to within a fraction of a pixel, and then co-adds the individual scans weighted by the signal-to-noise ratio.

The NGC 3067 absorption system is clearly detected in Mg II $\lambda\lambda$2795, 2803 and in Fe II $\lambda\lambda$2599 and 2586 at a redshift of $z = 0.005 \pm 0.001$. Although the low-dispersion *IUE* spectra do not resolve the various velocity components of this feature, we assume that the absorptions arise from all three systems in order to explain the large equivalent widths. In the LWP/LWR spectra, both of the Mg II doublet lines appear to be detected (splitting $\Delta\lambda = 7$ Å) at comparable strengths, consistent with saturation, although the low signal-to-noise ratio precludes a confident determination of relative line strengths. Note that Fe II λ2382 partially absorbs the red wing of the C IV λ1549 broad emission line in 3C 232, leading to an uncertain equivalent width estimate.

The most curious aspect of the LWP/LWR spectra is the apparent absence of Galactic absorption in the UV lines of Fe II and Mg II. In Figure 1 the Milky Way Ca II absorption has strength comparable to that in NGC 3067. In system 1, the Ca II and Na I doublet ratios suggest saturation, while the Galactic Ca II is unresolved and unsaturated. The Galactic Na I is seriously masked by the presence of telluric emission lines, but probably is also unsaturated. Higher resolution UV spectra will likely detect both the Galactic absorption and the other velocity components in NGC 3067. The equivalent width ratio Mg II/Ca II ≈ 13 for the total absorption profile, similar to values obtained for other low-z quasar absorption systems (Bergeron, D'Odorico, & Kunth 1984).

The SWP spectrum, also shown in Figure 3, does not show any absorption features due to NGC 3067. Upper limits are given in Table 2 for C IV, Si IV, Si II, and Lyα estimated from the 2 σ noise level in the adjacent continuum. Galactic Si II may have been detected, but the feature is near the end of the spectrum and close to a camera artifact at 1280 Å. The apparent emission line at 1280 Å is, in fact, a camera artifact (Hackney, Hackney, & Kondo 1982) resulting from a "hot spot" on the SWP camera detector. Bruhweiler et al. (1986) previously identified this feature as the 833 and 834 Å resonance lines of O II or O III, but if this feature were real it would be unexpected, since these lines would imply that portions of the broad-line clouds are optically thin in the Lyman continuum. To test the reality of this feature, we examined long exposures of blank sky, taken near 3C 232 and matched near in time to each of the SWP exposures in Table 1. These sky frames were then used to perform a sky subtraction of the 3C 232 SWP images. The 1280 Å feature did not appear at a statistically significant level in any of the three images or in the combined total. Therefore, we confirm neither the proposed detection of O II/O III resonance lines nor the other emission lines (C II, O VI) shortward of Lyα proposed by Bruhweiler et al. (1986).

Although the low redshift of NGC 3067 makes it difficult to separate Lyα absorption from geocoronal emission in *IUE* low-resolution spectra, we have attempted to detect its presence. The column of $N(\text{H I}) = 3.24 \times 10^{21}$ cm^{-2} detected in 21 cm emission toward 3C 232 (CvGS) should produce a damped Lyα absorption line of 42 Å equivalent width. We folded the unsaturated portion of the geocoronal Lyα emission line about its midpoint and subtracted the red side from the blue side. The predicted position of the Lyα absorption due to NGC 3067 is close, but not inside the saturated portion of geocoronal Lyα. No statistically significant Lyα absorption (4.5 ± 5.0 Å) was present at the correct position (1221.5 Å). In view of the large discrepancy between observations and predictions, we conclude that we were unsuccessful in avoiding geocoronal Lyα.

By a short extrapolation of the combined *IUE* (SWP) spectrum of 3C 232 in Figure 3*b*, we obtained a value of 5×10^{-15} ergs cm^{-2} s^{-1} Å^{-1} for the mean *observed* flux of 3C 232 at 912 Å. We also confirm the variability in the *IUE* fluxes reported by Bruhweiler et al. (1986). This implies variations in the 912 Å flux by a factor of 2 or more in one day, from (3–8) $\times 10^{-15}$ ergs s^{-1} cm^{-2} Å^{-1}. The (energy) spectral index was also observed to change from -1.4 to -3.6 in the *IUE* wavelength range (Bruhweiler et al. 1986). A brief (1679 s) exposure made with the *Einstein* Imaging Proportional Counter (IPC sequence No. 2172) detected 3C 232 at a flux level of 0.024 ± 0.008 μJy. This soft X-ray flux lies on an extrapolation of the mean *IUE* (SWP) spectrum to short wavelengths.

4. OPTICAL IMAGING

On 1989 March 6 and 7 we obtained direct imaging of the 3C 232/NGC 3067 system with the Kitt Peak National Observatory 2.1 m telescope equipped with a Tektronix 512 × 512 CCD camera with 27 μm square pixels, each subtending 0".34 in the focal plane of the telescope. The 512 × 512 format yields a usable field of view of 2'.6 × 2'.6. Owing to the low readout noise of 7.8 electrons, even the narrow-band images obtained are easily sky-limited.

The seeing during both of these photometric nights was excellent (0".8). Three separate images were obtained at each of two different locations: (1) the region of the H I finger between NGC 3067 and 3C 232 and (2) north of 3C 232 in the vicinity of the northern H I cloud that may have been detected by CvGS. This second pointing also encompassed most of the H I finger. Initially, a 10 minute broad-band image was taken through a Gunn *R* filter. Next, two 20 minute exposures were taken through a narrow (75 Å) interference filter whose bandpass would include any Hα and [N II] emission at the redshift of the 3C 232 absorption systems (filter 6606 in the KPNO redshifted Hα filter set; $\lambda_c = 6606$ Å; $\Delta\lambda = 75$ Å). Finally, a corresponding "off-band" image was obtained through a similar interference filter centered on the continuum $\sim$400 Å longward of Hα. The Hα "off-band" filter was chosen to avoid any potential [S II] emission from the H I clouds.

Spatial irregularities in all the images were removed by using flat-field calibration observations of a lamp projected on the telescope dome. The narrow-band images were scaled to each other, using the sky counts well away from the H I detections of CvGS, and were aligned using field stars and 3C 232. The Hα and off-band images were then subtracted to produce pure Hα images, shown in Figures 4*a* and 4*b* (Plate 1) at two contrast levels, along with the broad-band Gunn *R* image (Fig. 4*c* [Plate 2]) at low contrast. A reproduction of the H I emission contours overlaid upon a broad-band blue plate is also shown (Fig. 4*d* [Plate 2]) for orientation. Note that the H I map and its associated photograph are at a different scale, to show the possible H I detection to the north-northeast of 3C 232. Besides the prominent H II regions in the disk of NGC 3067 and the weak presence of 3C 232, owing to its very blue color relative

FIG. 4*a*

FIG. 4*b*

FIG. 4.—(*a*) Low-contrast optical image of the NGC 3067 and 3C 232 system in "pure Hα emission," minus the continuum, taken in a 40 minute exposure at the Kitt Peak 2.1 m telescope. The seeing is $\sim 0\rlap{.}''8$. (*b*) High-contrast image of the same Hα frame, showing the background level clearly. The bad CCD line above the disk was not used in the flux limits. (*c*) Ten minute frame taken with the Gunn *R* filter. (*d*) Contour map of H I overlaid on a broad-band blue image kindly provided by H. C. Arp. This image was previously published in CvGS and has a different field of view to include the possible northern cloud.

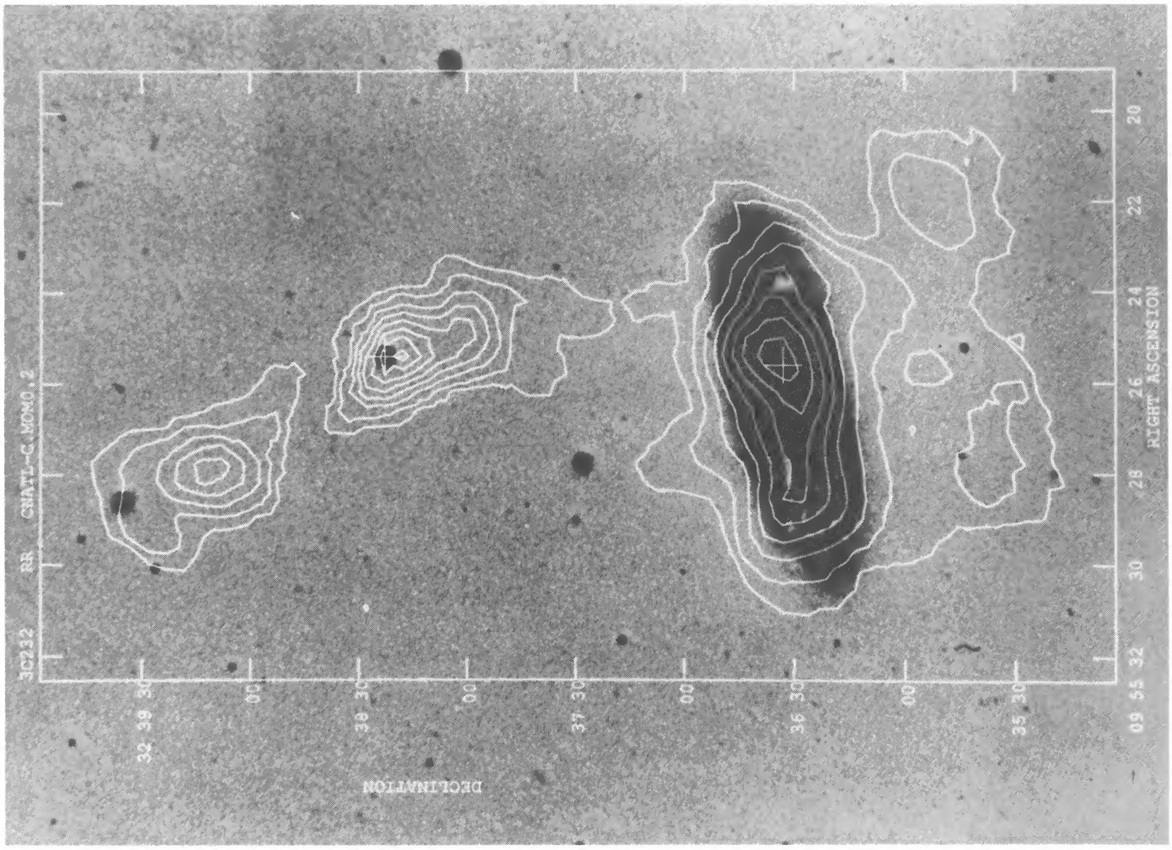

FIG. 4*d*

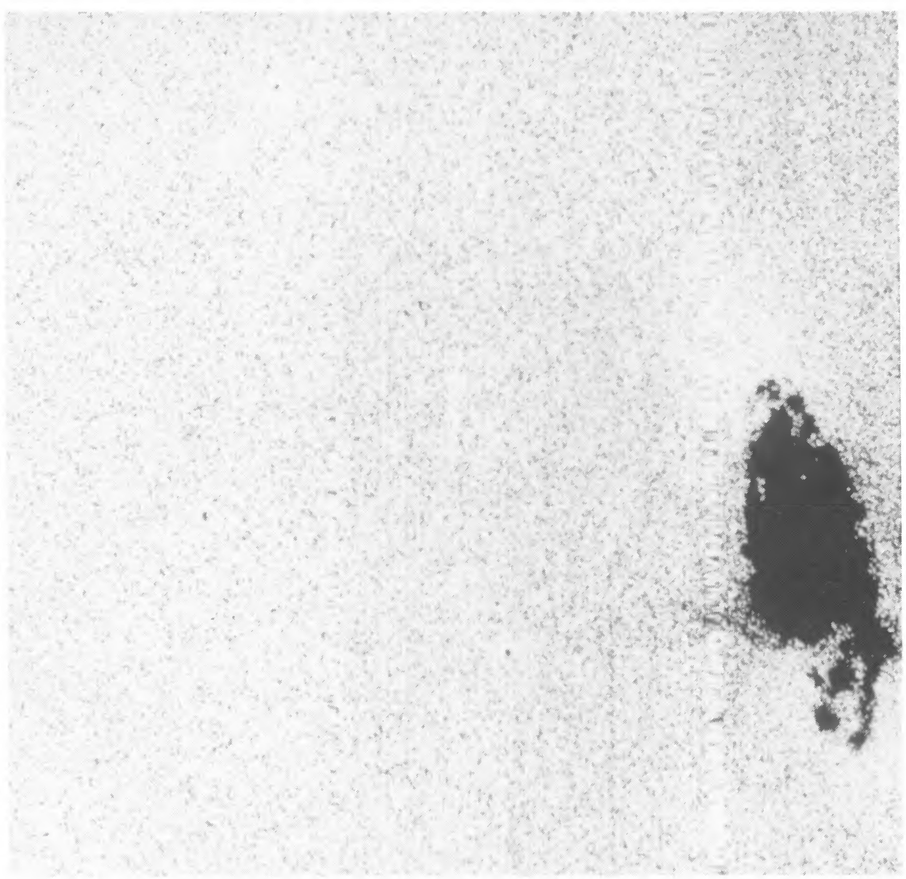

FIG. 4*c*

STOCKE et al. (see 374, 76)

to the sky, there is no evidence for Hα emission from the vicinity of the H I clouds discovered by CvGS. While there is no visual evidence on the high-contrast Hα image for any emission in the vicinity of the H I finger, some Hα emission is visible just north of the eastern edge of NGC 3067. This emission may be real or may be due to light scattered within the 2.1 m telescope optics and/or CCD Dewar window from the bright H II regions at the eastern edge of the disk of NGC 3067. This type of scattered-light problem complicates the detection of Hα emission immediately above the disks of highly inclined spiral galaxies (e.g. NGC 891 studied by Rand, Kulkarni, & Hester 1990), and it makes the interpretation of any possible detection highly problematical. Neither of the broad-band R images revealed continuum emission corresponding to the H I contours of CvGS, nor is 3C 232 resolved on our R-band images to a level of $\sim$23 mag arcsec^{-2}.

Flux calibration of the resultant images was accomplished using observations of the standard star Hiltner 600 (Stone 1977), providing absolute 3 σ upper limits on the presence of Hα. On the pure Hα image shown in Figure 4*b*, we measured the number of electrons in an area of the H I finger corresponding to the second-to-last contour of the H I map, with N(H I) $= 5.9 \times 10^{20}$ cm^{-2}. Since this area encompasses 3C 232 itself, we subtracted the number of counts attributed to the quasar and adjusted the number of sky pixels accordingly. Specifically, in 12,931 pixels we measured 2.84×10^4 electrons in 40 minutes. In the 441 pixels surrounding the quasar, we subtracted 2.08×10^4 electrons, leaving a net value of 7520 electrons in 12,490 pixels (3.4×10^{-8} sr) over 40 minutes. Because the formal noise (3 σ) in this area of sky is 11,252 electrons, we have a nondetection. If we add the values of the northern exposure, we get a formal noise of 16,427 electrons in 80 minutes of exposure. The bad CCD columns visible immediately north of NGC 3067 in Figure 4*b* were not used in determining these limits.

A similar analysis yields a net value of 64 electrons and a formal noise of 9913 electrons over 40 minutes in the 9400 pixels encompassing the H I cloud to the north. The formal noise standard deviations are consistent with the expectations from photon statistics alone, as long as the exposures are smoothed over at least 45 arcsec^2; systematics that may correspond to fringing effects create non-Gaussian errors on scales smaller than that. Since both H I emission regions cover many square arcminutes, the assumption of Poisson statistics is a good one.

Our nondetection on the H I finger converts to a flux limit f(Hα + [N II]) $< 1.3 \times 10^{-15}$ ergs cm^{-2} s^{-1} and to an intensity limit 3.8×10^{-8} ergs cm^{-2} s^{-1} sr^{-1}. Over the northern "cloud" our limit is 1.7×10^{-15} ergs cm^{-2} s^{-1}. These limits correspond to $\sim$27.5 mag arcsec^{-2} (3 σ) at each location. The limit on broad-band emission in the Gunn R band ($\lambda_c = 6555$ Å, $\Delta\lambda = 846$ Å) from any starlight that might be associated with the H I is 28.0 mag arcsec^{-2} (3 σ) for both the H I finger and the northern cloud.

As shown in Figure 4, the disk of NGC 3067 is filled with prominent H II regions, consistent with its identification as a "starburst" galaxy (CvGS) on the basis of its high integrated radio continuum flux and high 60 and 100 μm fluxes from the *Infrared Astronomical Satellite* (*IRAS*). As with the H I contours reported by CvGS and the radio continuum contours (Haxthausen, Carilli & van Gorkom 1990), the H II regions also show a marked asymmetry relative to the nucleus and to the dynamical center, marked with a plus sign in Figure 4*d*, of the galaxy based on the H I rotation curve of CvGS. The western side of the galaxy is significantly truncated. The galaxy appears to be missing an entire spiral arm, which, to be symmetrical with the southwestern arm clearly visible in the high-contrast Hα image, should extend outward from the northwest edge of the galaxy and trail to the west or southwest. This arm is missing in H I, in Hα, and in the radio continuum (Haxthausen, Carilli & van Gorkom 1990). We suggest that this arm is what has been detected in H I pointing toward 3C 232.

5. PHYSICAL CONDITIONS IN THE ABSORBING CLOUD

5.1. *Column Densities*

The optical observations of Na I and Ca II absorptions reported in § 2, can be used to determine a range of column densities for these species in all three velocity components. The limit of 3.7 km s^{-1} FWHM of the 21 cm absorption line (Wolfe 1979; RTF) translates to limits of $T \leq 300$ K and $b \leq 2.2$ km s^{-1} on the temperature and Doppler parameter of the cold H I gas, if the broadening is thermal. This gas could be as cold as 100 K if the 21 cm is broadened by turbulence or multiple components.

The strongest absorption lines occur in system 1, in which each line in the two doublets is detected. In Na I both D1 and D2 are saturated; although the weaker D1 line has a larger equivalent width than D2, the doublet ratio is unity within the measurement errors. In order for this to happen, the line-center optical depth of Na I D1 must exceed 2 or 3. In § 5.3 we will show that Na I probably occurs almost entirely in the cold H I, whereas Ca II occurs in comparable quantities in both cold and warm H I. If the Na and Ca Doppler parameters are thermal ($b \propto m^{-1/2}$), they could be as low as b(Na I) $= 0.5$ km s^{-1} and b(Ca II) $= 0.35$ km s^{-1}. However, the curves of growth suggest that the b-values are in the range 1–4 km s^{-1} (Na I) and 2–4 km s^{-1} (Ca II). Column densities were derived with standard curve-of-growth techniques with results given in Table 3. The minimum values are N(Na I) $\geq 1.1 \times 10^{12}$ cm^{-2} and N(Ca II) $\geq 1.5 \times 10^{12}$ cm^{-2}, based on a linear curve of growth for the Na D1 and Ca H lines, respectively. However, the lines are clearly saturated, and the actual columns are somewhat higher than these minimum values. The "best values," determined from minimum χ^2, are N(Na I) $= 2 \times 10^{12}$ cm^{-2} and N(Ca II) $= 3 \times 10^{12}$ cm^{-2}.

The ratio of N(Na I)/N(Ca II) in system 1 is between 0.7 and 1.7, depending on the curve of growth selected. This ratio is above the values seen in the Galactic halo and toward high-velocity clouds in the disk (Routly & Spitzer 1952; Siluk & Silk 1974), suggesting that the Ca-containing dust grains have not been strongly disturbed by shock waves. We will show later

TABLE 3

Na I AND Ca II COLUMN DENSITIES[a]

Column Density (cm^{-2})	System 1	System 2	System 3
N(Na I)	(1.1–10) $\times 10^{12}$	(2 ± 1) $\times 10^{11}$	($\leq 1.0 \pm 0.5$) $\times 10^{11}$
N(Ca II)	(1.5–6) $\times 10^{12}$	(2 ± 0.5) $\times 10^{11}$	(1 ± 0.3) $\times 10^{11}$
(Na I/Ca II)[b] ...	0.7–1.7	1	≤ 1

[a] All column densities assume single-component curve of growth, with $2 \leq b$(Ca II) ≤ 4 km s^{-1} and $1 \leq b$(Na I) ≤ 4 km s^{-1}, based on H I line widths and constraints from equivalent widths. The "best values" for Na I (2×10^{12} cm^{-2}) and Ca II (3×10^{12} cm^{-2}) in system 1 correspond to $b \approx 2$–3 km s^{-1}.

[b] Ratio of N(Na I)/N(Ca II), based on "best values" for $b \approx 2.2$ km s^{-1} for Na I and Ca II (system 1).

(§ 5.4) that the ratio of Na and Ca depletion factors is similar to those seen in low-velocity diffuse clouds in the Milky Way. For example, recent high-resolution observations (Crawford, Barlow, & Blades 1989) of 22 lines of sight toward the Sco OB1 association found $N(\text{Na I})/N(\text{Ca II}) \approx 2$–200 for "normal" low-velocity gas ($|v_{LSR}| < 20$ km s^{-1}), whereas $N(\text{Na I})/N(\text{Ca II})$ drops below 0.4 in intermediate-velocity clouds. The lack of significant depletion of elements such as Ca, Si, and Fe in interstellar clouds with $|v_{LSR}| > 50$ km s^{-1} (Shull, York, & Hobbs 1977) is usually interpreted (Cowie 1978; Shull 1978) as a result of grain destruction in hydromagnetic shocks. We will assume that refractory heavy elements in the H I cloud are depleted onto grains in proportions similar to those in the Milky Way.

In systems 2 and 3, we derive comparable columns of Ca II and Na I, within the uncertainties of the measurements. These components were assumed to lie on the linear portion of the curve of growth. Here too, the Na I/Ca II ratios of unity suggest that little disruption of grains has occurred.

The low-resolution *IUE* data on Mg II and Fe II are unable to provide reliable column densities because of line saturation. However, the large equivalent widths (5–6 Å) can only result if these species are spread out in velocity by ~ 150 km s^{-1}, comparable to the range of Ca II and Na I components shown in Table 2.

5.2. *Inferences from the Imaging Data*

In the H I finger coincident on the sky with 3C 232, with solid angle $\Omega = 3.4 \times 10^{-8}$ sr, there is no detectable Hα emission to a limit of $f(\text{H}\alpha + [\text{N II}]) = 1.3 \times 10^{-15}$ ergs cm^{-2} s^{-1}, assuming Poisson noise (3 σ). The surface brightness limit is therefore $f/\Omega = 3.8 \times 10^{-8}$ ergs cm^{-2} s^{-1} sr^{-1}. We can convert these measurements to a limit on the ionizing photon flux, if we assume that any observable Hα emission results from recombination of hydrogen ionized by a photon flux Φ_{ion}.

If the Hα emission is optically thin, statistical equilibrium limits the ionizing photon flux to

$$\Phi_{\text{ion}} = \left[\frac{0.75 f(\text{H}\alpha + [\text{N II}])}{\Omega}\right]\left[\frac{4\pi\alpha_B}{\epsilon(\text{H}\alpha)}\right]\left(\frac{A_{\text{proj}}}{A_{\text{tot}}}\right)$$

$$= (6.86 \times 10^5 \text{ cm}^{-2}\text{ s}^{-1}) f_{-15}\Omega_{-8}^{-1}\left(\frac{A_{\text{proj}}}{A_{\text{tot}}}\right), \quad (1)$$

where $\alpha_B = 2.59 \times 10^{-13}$ cm^3 s^{-1} is the hydrogen recombination coefficient and $\epsilon(\text{H}\alpha) = 3.56 \times 10^{-25}$ ergs cm^3 s^{-1} is the Hα emission rate coefficient for case B at 10^4 K (Osterbrock 1989). Here f_{-15} is the limit on the Hα + [N II] flux from the H I cloud in units of 10^{-15} ergs cm^{-2} s^{-1}, and Ω_{-8} is the angular size of the cloud in units of 10^{-8} sr. We also assumed an intensity ratio Hα/(Hα + [N II]) = 0.75. The last factor is the ratio of the cloud's projected area to total area, equal to $\frac{1}{2}$, $1/\pi$, or $\frac{1}{4}$ for a two-sided slab, a long cylinder, and a sphere, respectively. For the cylindrical geometry, and the observed values ($f_{-15} = 1.3$ and $\Omega_{-8} = 3.4$), we find $\Phi_{\text{ion}} < 8.35 \times 10^4$ cm^{-2} s^{-1}.

The corresponding limit on specific intensity at 13.6 eV depends on whether the incident radiation field is direct or diffuse. For a diffuse isotropic radiation field, such as that from the extragalactic background, the effective solid angle irradiating the 3C 232 cloud is π sr, since the cloud is optically thick in the Lyman continuum and irradiated from one side only. If we set $I_\nu = I_0(\nu/\nu_0)^{-s}$, where $s > 0$ and $h\nu_0 = 13.6$ eV, and consider only the ionizing flux between 1 and 4 rydbergs, then $\Phi_{\text{ion}} = (\pi I_0/h)[(1 - 4^{-s})/s]$. The limit on diffuse specific intensity at 13.6 eV is then

$$I_\nu(13.6 \text{ eV}) < (1.45 \times 10^{-21} \text{ ergs cm}^{-2}\text{ s}^{-1}\text{ Hz}^{-1}\text{ sr}^{-1}) \times \left(\frac{A_{\text{proj}}}{A_{\text{tot}}}\right) f_{-15}\Omega_{-8}^{-1}\left(\frac{s}{1 - 4^{-s}}\right). \quad (2)$$

If $s = 0$ the last term in parentheses, involving the spectral index s, should be replaced with $(\ln 4)^{-1}$. Notice that this limit does not depend upon any physical quantity associated with the cloud (e.g. density or volume), given the assumption of optically thin Hα. If we assume a flat diffuse spectrum between 1 and 4 rydbergs ($s = 0$) and cylindrical cloud geometry, we obtain an upper limit $I_0 = I_\nu(13.6 \text{ eV}) < 1.8 \times 10^{-22}$ ergs cm^{-2} s^{-1} Hz^{-1} sr^{-1}, independent of the Hubble constant. The limit is a factor of 1.85 times higher for $s = 1$.

Because hot stars in the nearby galaxy NGC 3067 may contribute to this ionizing flux, this value is an upper limit on the UV background flux due to extragalactic sources (Sargent et al. 1980; Bechtold et al. 1987). Our limit from Hα is somewhat larger than recent models (Bechtold et al. 1987) for the UV background, which suggest values around 10^{-23} ergs cm^{-2} s^{-1} Hz^{-1} sr^{-1} at the current epoch based upon the integrated light from local Seyfert galaxies. Fabry-Perot experiments performed by Songaila, Bryant, & Cowie (1989) on high-velocity clouds in our own Galaxy's halo give upper limits on the cosmic ionizing flux of 6×10^{-23} ergs cm^{-2} s^{-1} Hz^{-1} sr^{-1} at the Lyman limit. Significantly longer integrations through narrower passband filters than those employed here could substantially decrease the limits on Hα emission from nearby intergalactic H I clouds such as this one, or from the intergalactic cloud in the M96 group recently studied by Schneider (1985, 1989). From equation (2) we also note that nearby clouds subtending a much larger solid angle on the sky offer the opportunity to set better limits on I_ν(13.6 eV) and may eventually provide a direct measurement of its value at the current epoch.

5.3. *Inferences from the* Na I *and* Ca II *Data*

Both Na I and Ca II can be photoionized by ultraviolet radiation at wavelengths longward of the 912 Å Lyman limit. Threshold energies of their valence shells are 5.138 eV (Na I) and 11.868 eV (Ca II). Because Na I and Ca II are minority "recombination species" compared with the dominant ionization stages Na II and Ca III, we may use the observations of Na I, Ca II, and H I to constrain the ionizing radiation field incident on the H I cloud.

The 21 cm absorption column density can be derived either by integrating the line optical depth over velocity,

$$N(\text{H I}) = (1.823 \times 10^{13} \text{ cm}^{-2}) T_{\text{spin}} \int \tau_v \, dv , \quad (3)$$

or by using the optical depth at the center of the resolved 21 cm line,

$$\tau_0 = (5.49 \times 10^{-14})\left[\frac{N(\text{H I})}{\pi^{1/2} b T_{\text{spin}}}\right], \quad (4)$$

for N in cm^{-2}, b in cm s^{-1}, and T in K. For a Gaussian profile, the integrated optical depth equals 1.064(FWHM)τ_0. RTF quote a line-center optical depth $\tau_0 = 0.027 \pm 0.0018$, a FWHM of 3.7 km s^{-1} ($b = 2.23$ km s^{-1}), and an integrated optical depth of 0.211 km s^{-1}. We believe that the quoted integrated optical depth is too large by a factor of 2; a value of 0.106 km s^{-1} is consistent with the observed line profile and τ_0. We then derive N(H I) = (1.93 × 10^{20} cm^{-2})T_3, where T_3 is the spin temperature in units of 10^3 K. From the 21 cm line width and Galactic studies of interstellar H I, $T_{\rm spin}$ is probably in the range 100–300 K.

As mapped by CvGS, the cloud in front of 3C 232 has an angular extent of about 0'.6 by 0'.9, which we approximate as a cylinder of diameter $D = (2.5 \text{ kpc})h^{-1}$ and length $L = (4 \text{ kpc})h^{-1}$. Toward 3C 232, which also corresponds to the peak of 21 cm emission, the H I column density is about 3.24 × 10^{21} cm^{-2} and the average H I density is n(H I) = (0.42 cm^{-3})h. Thus, the cold H I absorption column of (1.93 × 10^{20} cm^{-2})T_3 represents 1%–2% of the total H I. We believe that this situation is most easily explained if the H I cloud consists of two phases: cold clouds at $T \leq 300$ K embedded in a lower density warm medium at $T \approx 8000$ K. The warm H I is not strongly absorbing at 21 cm and is commonly seen in emission throughout the Milky Way (Dickey et al. 1983). From limits on the 21 cm optical depth in the line wings, the bulk of the cloud must be warm ($T > 10^3$ K). It is possible that, because of the 3' Arecibo beam, emission from the H I cloud fills in the absorption in the wings. However, the two-phase interpretation has also been suggested by Briggs & Wolfe (1983) to explain systems that show absorption at both 21 cm and Mg II. We will henceforth assume that the cold and warm components have $T_c = 300$ K and $T_w = 8000$ K, respectively.

Because the sound crossing time of the warm H I cloud is just (2 × 10^8 yr)h^{-1}, pressure equilibrium is probably achieved between the cold "clouds" and the warm "intercloud" H I. Thus, we set $n_{\rm H} T = n_c T_c = n_w T_w = (3360 \text{ cm}^{-3} \text{ K})h$, or $n_{\rm H} = (3.36 \text{ cm}^{-3})hT_3^{-1}$. At our adopted temperatures, the clouds have a density $n_{\rm H} = (11.2 \text{ cm}^{-3})h$, and the intercloud gas has $n_{\rm H} = (0.42 \text{ cm}^{-3})h$. We set the electron density equal to $n_e = (5 \times 10^{-4})n_{\rm H}$ (Spitzer 1978), appropriate for a neutral cloud in which the free electrons are donated by trace elements such as C, Mg, Si, S, and Fe ionized by UV radiation of energy below 1 rydberg.

Using the equations of photoionization equilibrium, we may solve for the ionization ratios,

$$\frac{N(\text{Na II})}{N(\text{Na I})} = \frac{\Gamma(\text{Na I})}{n_e \alpha(\text{Na I})} = (20.8)I_{-23}\, T_3^{1.80} h^{-1} , \qquad (5)$$

$$\frac{N(\text{Ca III})}{N(\text{Ca II})} = \frac{\Gamma(\text{Ca II})}{n_e \alpha(\text{Ca II})} = (1.25)I_{-23}\, T_3^{1.75} h^{-1} . \qquad (6)$$

Here α is the recombination rate coefficient (cm^3 s^{-1}) *to* the stated ion state, and Γ is the photoionization rate (s^{-1}) *from* that ion state. We assumed an isotropic radiation field $I_\nu = I_0(\nu/\nu_0)^{-1}$, where the intensity at the Lyman limit, $h\nu_0 = 13.6$ eV, is written $I_0 = (10^{-23} \text{ ergs cm}^{-2} \text{ s}^{-1} \text{ Hz}^{-1} \text{ sr}^{-1})I_{-23}$. From Aldrovandi & Péquignot (1974) we fit α(Na I) = (1.02 × 10^{-12} cm^3 s^{-1})$T_3^{-0.80}$ and α(Ca II) = (5.16 × 10^{-12} cm^3 s^{-1})$T_3^{-0.75}$ over the temperature range $2.0 \leq \log T \leq 4.0$. For photoionization rates we derived the formulae Γ(Na I) = (3.56 × 10^9 s^{-1})I_0 and Γ(Ca II) = (1.08 × 10^9 s^{-1})I_0, based on the integrals,

$$\Gamma_i = 4\pi \int_{\nu_T}^{\infty} \left(\frac{I_\nu}{h\nu}\right) \sigma_i(\nu) d\nu , \qquad (7)$$

where $h\nu_T$ is the threshold ionization energy of the valence shell, and $\sigma_i(\nu)$ is the photoionization cross section. The steep temperature dependence in the ion ratios arises from the recombination rate, $n_e \alpha(T)$, and the assumption of pressure equilibrium, with constant nT.

The photoionization integrals assumed an isotropic radiation field, since the Na I and Ca II edges lie below 13.6 eV. A more sophisticated calculation is required to treat the effects of radiation in the Lyman continuum. For a direct ionizing flux, one replaces $4\pi I_\nu$ by F_ν. For Na I we used cross sections of Reilman & Manson (1979), supplemented by Hudson & Carter (1967) to cover the "Cooper minimum" region from threshold ($h\nu_T = 5.138$ eV) to 6.000 eV. For Ca II we used cross sections from Reilman & Manson (1979), supplemented by Black, Weisheit, & Laviana (1972) from threshold ($h\nu_T = 11.868$ eV) to 25 eV.

We can now use the equations of photoionization equilibrium (eqs. [5] and [6]) together with the formulae for α and Γ to solve for the ionizing radiation intensity, I_{-23}. Let N_1 and N_2 denote the column densities of the first and second ion stages of an element (here Na I and Na II; or Ca II and Ca III). If we write $\Gamma = AI_{-23}$, $\alpha = BT_3^{-s}$, and $n_e = (5 \times 10^{-4})n_{\rm H} = CT_3^{-1}$, and if we assume that $(N_1 + N_2) = \zeta d N_{\rm H}$, where ζ and d are the abundance and depletion factors, respectively, then the solutions to the ionization and abundance equations are given by

$$\frac{N_2}{N_1} = \left(\frac{A}{BC}\right) T_3^{(1+s)} I_{-23} , \qquad (8)$$

$$I_{-23} = \left[\left(\frac{\zeta d N_{\rm H}}{N_1}\right) - 1\right]\left(\frac{BC}{A}\right) T_3^{-(1+s)} . \qquad (9)$$

When we substitute equation (9) in equation (8), we recover the obvious relation

$$\frac{N_2}{N_1} = \left[\left(\frac{\zeta d N_{\rm H}}{N_1}\right) - 1\right] . \qquad (10)$$

No solution is possible if $\zeta d < (N_1/N_{\rm H})$, since one then lacks sufficient amounts of the element in the gas phase to explain the observed values, N_1 and $N_{\rm H}$. This limits the depletion factors, d, to values greater than $(N_1/\zeta N_{\rm H})$.

In our case, we assume that the Na and Ca in the H I cloud are depleted from their cosmic values, Na/H = 2.14 × 10^{-6} and Ca/H = 2.29 × 10^{-6}, by factors $d_{\rm Na}$ and $d_{\rm Ca}$. For the Milky Way (Phillips, Pettini, & Gondhalekar 1984) the mean depletion factor of Na is $d_{\rm Na} = 0.25$, independent of mean density, whereas Ca is observed to be more depleted with increasing cloud density. At the average density of the H I cloud, $n_{\rm H} = (0.42 \text{ cm}^{-3})h$, one would expect $d_{\rm Ca} \approx 10^{-2.5}$. However, it is likely that the metallicity and dust-to-gas ratio in this cloud are less than in the Galaxy (see § 5.4). We have therefore adopted fiducial depletion factors of $d_{\rm Na} = 0.25$ and $d_{\rm Ca} = 0.10$.

For N(H I) = (1.93 × 10^{20} cm^{-2})T_3, and the "best values" of the observed column densities, N(Na I) = 2 × 10^{12} cm^{-2} and N(Ca II) = 3 × 10^{12} cm^{-2}, the solutions are

$$I_{-23}(\text{Na}) = (0.0481)h\left[(51.6)T_3\left(\frac{d_{\rm Na}}{0.25}\right) - 1\right] T_3^{-1.80} , \qquad (11)$$

$$I_{-23}(\text{Ca}) = (0.803)h\left[(14.7)T_3\left(\frac{d_{\rm Ca}}{0.10}\right) - 1\right] T_3^{-1.75} . \qquad (12)$$

As noted above, no solutions at $T = 300$ K are possible if $d_{\rm Na} < 0.016$ or if $d_{\rm Ca} < 0.023$. Our choices of fiducial depletion factors are therefore sensible.

One can demonstrate that the column density of Na I is dominated by the cold gas, while Ca II forms in both cold and warm gas. For a two-component model with 5.8×10^{19} cm^{-2} of cold H I at 300 K and 3.24×10^{21} cm^{-2} of warm H I at 8000 K, and for $I_{-23} \geq 1$ and $0.5 < h < 1$, Na II is the dominant ion stage in the 300 K clouds, but Ca II and Ca III have comparable ion fractions. If we set N(Na I) and N(Ca II) equal to their "best values," the solutions to equations (8) and (9) at 300 K are $I_{-23} = 6.1h$ and N(Na II)/N(Na I) = 14.5 from Na I; and $I_{-23} = 23h$ and N(Ca III)/N(Ca II) = 3.4 from Ca II. The value of the radiation field for Na I is below the limit, $I_{-23} < 18$, set by the absence of Hα emission toward the H I cloud. The Ca II value would probably be lower also, if we accounted for the Ca II formed in the warm H I. Furthermore, the Ca depletion might be lower than the assumed factor $d_{\rm Ca} = 0.1$. At the maximum of their curve-of-growth range, we have N(Na I) $= 10^{13}$ cm^{-2} and N(Ca II) $= 6 \times 10^{12}$ cm^{-2}, which correspond to values of $I_{-23} = 0.88h$ (Na) and $I_{-23} = 8h$ (Ca).

These calculations demonstrate the sensitivity of absorption-line measurements to small columns of trace elements. To take the method any further, however, we need more refined models of the temperature, density, and ionization in the cloud-intercloud medium. It would also be useful to determine the curves of growth more accurately, to decrease the range of column densities, particularly for Na I.

5.4. *Evidence for Grains and Depletion*

In the previous section we tacitly assumed the existence of dust grains in the H I cloud, and used mean depletion factors $d_{\rm Na} = 0.25$ and $d_{\rm Ca} = 0.1$. The observed ratio of Na I/Ca II column densities is consistent with depleted gas, since $d_{\rm Na}/d_{\rm Ca}$ is typically 80 in the Galactic interstellar medium (Phillips et al. 1984) for $n_{\rm H} \approx 0.42h$ cm^{-3}. However, the calculations of ionization equilibrium described in the previous section limit $d_{\rm Na}$ and $d_{\rm Ca}$ to values greater than about 0.02. This is certainly expected to be the case for Na, but it does constrain the amount of Ca depletion to be less than typical for the Milky Way.

Thus, there is fair circumstantial evidence for grains in the H I cloud toward 3C 232. However, the metallicity and dust-to-gas ratio in the H I cloud probably differ from the Galactic values. Recent studies of the Galactic interstellar medium (ISM) (Shull & Van Steenberg 1985) find $\langle N({\rm H\ I})/E(B-V)\rangle = 5.2 \times 10^{21}$ cm^{-2} mag^{-1}, suggesting that 3C 232 should have a reddening $E(B-V) \approx (0.62)D$, where D is the dust-to-gas ratio, by mass, relative to the Galactic interstellar value of 0.0075 (Spitzer 1978). The *IUE* spectrum of 3C 232 (Fig. 5) in the vicinity of the 2175 Å extinction feature sets a limit on extinction $E(B-V) \leq 0.2$, implying that $D < 0.3$. Because the 2175 Å feature is normally attributed to graphite grains, this limit may not apply to the grains containing Ca and Na. However, the lack of this feature does raise a concern that the Na and Ca abundances adopted in § 5.3 might be too large by a factor of 3, if the grain abundance is proportional to metallicity. Alternatively, grain formation may not have been as extensive in this cloud as in the local ISM. The derived values of the radiation field, I_0, are proportional to the adopted abundances and the depletions of Na or Ca. Thus, a lower value of either parameter translates to a lower limit on the ionizing radiation. Additional UV absorption measurements of depleted and undepleted species with the *Hubble Space Telescope* might resolve this question.

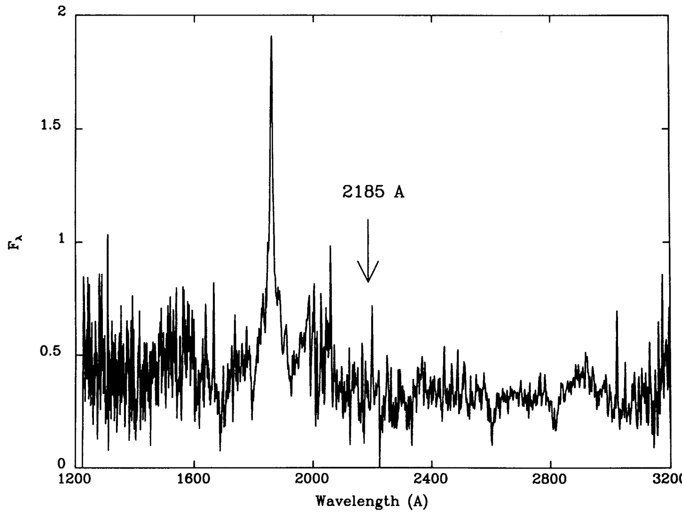

FIG. 5.—Combined *IUE* (SWP 25496 and LWR 17661) low-resolution spectra of 3C 232, showing F_λ (ergs cm^{-2} s^{-1} Å^{-1}). The data were taken on 1985 March 20 and 21, were reduced by Gaussian extraction, and show the continuum near the 2175 Å extinction feature (2185 Å observed frame). The two spectra are joined at 1982.8 Å. No evidence for a grain feature can be seen, to a limit of $E(B-V) \leq 0.2$ for a Galactic selective extinction curve.

6. REDSHIFT-INDEPENDENT DISTANCE ESTIMATE FOR 3C 232

Because the apparent association of 3C 232 and NGC 3067 was one of only four pairs of 3C quasars and NGC galaxies providing strong statistical support for the "noncosmological redshift" hypothesis for quasars (e.g., Arp 1987), it is worthwhile to consider that hypothesis in the light of this new information. Indeed, if the H I map of CvGS had been published 15 years ago, it would have been viewed as extremely strong evidence in favor of noncosmological redshifts. However, we note that CvGS observed the 3C 232/NGC 3067 system in H I emission specifically because 3C 232 was previously known to possess H I absorption at the redshift of NGC 3067. So, while the H I cloud was expected to be present, it was only the morphology that was unknown and unexpected, not the coincidence of the H I emission with the quasar position.

It is possible to examine the redshift hypothesis using our nondetection of Hα recombination radiation from the H I cloud to constrain the minimum distance of quasar 3C 232 from the cloud. At nearer distances, the ionizing flux seen from the quasar in the ultraviolet would ionize the hydrogen in the cloud, emitting Hα photons as it recombined. This argument is true even if the quasar ionizing radiation is beamed, unless the beam opening angle is much smaller than beam sizes suggested for QSOs (Barthel 1989) and intercepts only a tiny portion of the observed H I cloud. That 3C 232 is situated near the peak of the H I column density contours argues against this interpretation because a very collimated beam of radiation would ionize the H I immediately surrounding 3C 232, causing a local minimum in H I column density at that position, contrary to observation. The argument below does not resort to any redshift information for the quasar, although the distance of (14.7 Mpc)h^{-1} to NGC 3067 and its associated H I cloud are obtained assuming the Hubble relation. The quasar cannot be embedded in the H I cloud (CvGS; Pesch, Westpfahl, & Simkin 1990) because the Strömgren sphere surrounding the quasar would be larger than the observed diameter of the H I cloud, causing it to be completely ionized.

A minimum distance can be inferred from the upper limit on Hα radiation from the cloud by assuming that all the ionizing flux comes from the quasar 3C 232. This ionizing flux can be found by a small extrapolation of the *IUE* SWP observations of 3C 232 listed in Table 1, giving a mean flux at the Lyman edge of 5×10^{-15} ergs s^{-1} cm^{-2} Å^{-1}. Bruhweiler et al. (1986) have reported that both the emission lines and the continuum appear to vary in this quasar on time scales of 1 month and 1 day, respectively, and that the continuum slope changes from $s = -1.4$ to $s = -3.6$. Since the recombination time scale in the ionized layer of the H I cloud that emits Hα is of order $(3 \times 10^5\ \mathrm{yr})h^{-1}$, the ionization state in the H I cloud would be set by the maximum quasar ionizing flux over the past 10^5 yr. For the purposes of this calculation we use the maximum SWP flux observed by Bruhweiler et al. (1986) and $s = -1.4$ to obtain an estimated $F_\lambda(912\ \text{Å}) = 8 \times 10^{-15}$ ergs cm^{-2} s^{-1} Å^{-1} or $F_\nu = 2.2 \times 10^{-27}$ ergs cm^{-2} s^{-1} Hz^{-1}.

In § 5 we derived limits on the ionizing photon flux, Φ_{ion}, or the diffuse specific intensity, I_0, at 13.6 eV from the lack of Hα emission over the H I cloud and from the Na I and Ca II ionization equilibria. If we assume that 3C 232 lies at a distance $R = (14.7\ \mathrm{Mpc})h^{-1}$, comparable to that of NGC 3067 and the H I cloud, the QSO's spectral luminosity is $L_\nu = 4\pi R^2 F_\nu$. We can then derive the minimum distance r of 3C 232 from the cloud by relating Φ_{ion} or $4\pi I_0$ to the ionizing fluxes on the H I cloud from a quasar located at a noncosmological distance. From the Hα limit and for an ionizing spectrum with energy spectral index $s = 1$, we find

$$r = (14.7\ \mathrm{Mpc})h^{-1}\left[\frac{0.75F_0(13.6\ \mathrm{eV})}{h\Phi_{\text{ion}}}\right]^{1/2} . \qquad (13)$$

From our observed values, $\Phi_{\text{ion}} < 8.35 \times 10^4$ cm^{-2} s^{-1} and $F_0 = 2.2 \times 10^{-27}$ ergs cm^{-2} s^{-1} Hz^{-1}, we find $r > (25\ \mathrm{kpc})h^{-1}$ from Hα.

From the Na I and Ca II limits on specific intensity, I_{-23}, the quasar must lie at a distance

$$r > (14.7\ \mathrm{Mpc})h^{-1}\left(\frac{F_\nu}{4\pi I_\nu}\right)^{1/2} = (61.5\ \mathrm{kpc})h^{-1}I_{-23}^{-1/2} \qquad (14)$$

from the H I cloud. If we use the "best values" for the Na I column densities, we find a limit $I_{-23} = 6.1h$ and a limiting distance $r(\mathrm{Na}) = (25\ \mathrm{kpc})h^{-3/2}$. If the Na I column density lies at the maximum of its range, so that $I_{-23} = 0.88h$, then we find $r(\mathrm{Na}) = (66\ \mathrm{kpc})h^{-3/2}$.

Our Hα lower limit on distance, $r \approx (25\ \mathrm{kpc})h^{-1}$, is larger by a factor of 3–7 than the values derived by Pesch et al. (1990), although their limiting flux, $f(\mathrm{H}\alpha) < 1.1 \times 10^{-15}$ ergs cm^{-2} s^{-1}, is comparable to our limit. There are several reasons for our larger distance limit. First, and most significantly, we measured the Hα flux limit over a 4 times larger angular cloud size. Second, we scaled our calculations with a Hubble constant of $h = (H_0/100)$. Third, we assumed that the largest flux observed from the quasar would determine the ionization balance in the cloud. The recombination time in the cloud is substantially longer than the time for variability in the quasar flux, thus effectively freezing in the maximum ionization induced in the cloud. This accounts for a factor of 2 in the ionizing flux. We also assumed that 25% of the emission near Hα would have been produced by [N II]. When all of these effects are taken into account, our upper limits are 3–7 times larger than theirs, as reported.

However, the limits on the radiation field provided by the ionization equilibrium of Na I are even lower than the Hα limit. Resonance absorption lines are more sensitive to small column densities than optical emission lines; thus, the absorption lines provide the best limits on the ionizing fluxes.

7. CONCLUSIONS

We have presented new optical spectra and imaging and have analyzed existing *IUE* ultraviolet spectra for the 3C 232/NGC 3067 system. These new observations add important constraints on the physical nature of the gas cloud near NGC 3067 that gives rise to the observed H I and metal absorption systems.

High-resolution optical spectra of 3C 232 show three separate velocity systems near the redshift of NGC 3067 but separated by 160 km s^{-1}. This large velocity spread is similar to, but not as large as, that seen in clumps of C IV absorbers at high redshift (York et al. 1986). Given that the morphology of the absorbing cloud is now known (CvGS) to be a finger of H I reminiscent of "tidal tails" in galaxy-galaxy interactions, some quasar metal-line systems at high redshift could be produced by gas stripped from spiral galaxies in interacting systems. The stripped gas effectively increases the cross section for absorption lines, and, if similar to the tidal tail near NGC 3067, could also account for the large velocity spread in the C IV lines. It is peculiar, however, that there is currently no evidence for a stellar tidal tail or for a galactic companion.

The velocity system showing the strongest lines of Ca II and Na I is coincident with the H I (21 cm) absorption at 1420 km s^{-1}. All three systems have low ratios of Na I/Ca II, although only in system 1 is this ratio well determined, N(Na I)/N(Ca II) ≈ 1. This low ratio suggests that the grains in this cloud have not been extensively processed by shocks or disturbed in any tidal stripping from NGC 3067. An analysis of the Na and Ca depletions shows that they are in a ratio similar to values in the Galactic interstellar medium. The lack of a 2175 Å grain extinction feature toward 3C 232 suggests that the grain-to-gas ratio is lower in the H I cloud than in the Milky Way by at least a factor of 3. This would decrease the limits on I_0 proportionally.

Ultraviolet (*IUE*) spectra show Mg II and Fe II absorption lines in 3C 232 at the redshift of NGC 3067 and place upper limits on the presence of C IV, Si IV, Si II, and Lyα. Although these data add little of physical significance, owing to the relatively low spectral resolution and low signal-to-noise ratio, this absorption system could have been discovered by *IUE* if it had not previously been known. A search for previously unknown absorption systems is now underway using the *IUE* archives, with limiting equivalent widths ~ 0.5 Å. The SWP spectra also allow us to estimate the ionizing flux from 3C 232 via a short extrapolation to the Lyman limit.

Optical CCD images were obtained of the area of the H I finger and the possible H I cloud north-northeast of 3C 232. No broad-band R or Hα + [N II] emission is visible in the area of the H I contours down to quite low limits (27.5 mag arcsec^{-2}). The absence of detectable emission at other wavelengths is similar to the circumstance for the H I "ring" seen in the M96 galaxy group (Schneider 1985, 1989) and suggests that the M96 ring may also be gas stripped from galaxies during an encounter.

The absence of Hα emission from the H I finger sets a 3 σ upper limit of $I_0 < (1.8\text{–}3.3) \times 10^{-22}$ ergs s^{-1} cm^{-2} Hz^{-1} sr^{-1} on the specific intensity of extragalactic radiation at the Lyman limit, assuming $I_\nu = I_0(\nu/\nu_0)^{-s}$, with $s = 0$ and 1, respectively. This limit does not depend on any characteristics of the H I cloud, except for its angular size, and can be improved upon with longer integration Hα imaging on nearby intergalactic clouds of greater observed angular size. The present limit is an order of magnitude greater than models of the expected extreme ultraviolet background from Seyfert galaxies (Bechtold et al. 1987), but of the same magnitude as upper limits derived from high-velocity clouds in the Galactic halo (Songaila et al. 1989).

Our studies of the Na I and Ca II ionization equilibrium in the H I cloud give a limit on the ionizing flux even lower than that obtained from Hα, but they depend on the metallicity and depletion of Na and Ca, and they are limited in accuracy by the curve of growth for saturated lines. Further optical and UV spectral measurements of 3C 232 at high resolution and high signal-to-noise ratio would be quite helpful, in order to determine the metal abundances, depletion factors, and grain characteristics in the H I cloud.

The two estimates of the UV ionizing flux on the H I finger, together with the observed UV flux from 3C 232, show that the quasar must lie a significant distance from the H I cloud,. The Hα limit places 3C 232 at least (25 kpc)h^{-1} away, and the Na I limit places the QSO at least (25–66 kpc)$h^{-3/2}$ from the H I cloud, independent of redshift information about the QSO. These limits require that the quasar must lie well behind the cloud, as seen from Earth, and thus makes it difficult kinematically for the quasar to be the cause of the tidal tail. We conclude that the quasar and the H I cloud are a chance projection, regardless of the true distance to 3C 232. Therefore, the H I finger provides no additional support for the non-cosmological redshift hypothesis.

This work was supported by grants from NASA/*IUE* (NAG5-193), NSF (AST87-15983), and the NASA Astrophysical Theory Program (NAGW-766) at the University of Colorado. The *IUE* analysis was carried out at the Colorado Regional Data Analysis Facility. M. E. D. acknowledges support of a NASA Graduate Researcher Fellowship. We thank Jacqueline van Gorkom, Chris Carilli, and Art Wolfe for helpful discussions during the course of this work, and George Sonneborn for helpful advice regarding the *IUE* hot pixel masquerading as O II/O III λ834.

REFERENCES

Aldrovandi, S. M. V., & Péquignot, D. 1974, Rev. Brasileira Fis., 4, 491
Arp, H. C. 1987, Quasars, Redshifts, and Controversies (Berkeley: Interstellar Media)
Barthel, P. D. 1989, ApJ, 336, 606
Bechtold, J., Weymann, R. J., Lin, Z., & Malkan, M. A. 1987, ApJ, 315, 180
Bergeron, J., D'Odorico, S., & Kunth, D. 1984, A&A, 180, 1
Bergeron, J., Savage, B. D., & Green, R. F. 1987, in Exploring the Universe with the *IUE* Satellite, ed. Y. Kondo (Dordrecht: Reidel), 703
Black, J. H., Weisheit, J. C., & Laviana, E. 1972, ApJ, 177, 567
Blades, J. C., Hunstead, R. W., & Murdoch, H. W. 1981, MNRAS, 194, 669
Boksenberg, A., Danziger, I. J., Fosbury, R. A. E., & Goss, W. M. 1980, ApJ, 242, L145
Boksenberg, A., & Sargent, W. L. W. 1978, ApJ, 220, 42 (BS)
Briggs, F. H., & Wolfe, A. M. 1983, ApJ, 268, 76
Bruhweiler, F. C., Kafatos, M., & Sofia, U. J. 1986, ApJ, 303, L31
Burbidge, E. M., Burbidge, G. R., Solomon, P. M., & Strittmatter, P. A. 1971, ApJ, 170, 233
Burbidge, E. M., et al. 1988, BAAS, 20 (No. 4), 741
Carilli, C. L., van Gorkom, J. H., & Stocke, J. T. 1989, Nature, 338, 134 (CvGS)
Cowie, L. L. 1978, ApJ, 225, 887
Crawford, I. A., Barlow, M. J., & Blades, J. C. 1989, ApJ, 336, 212
Dickey, J. M., Kulkarni, S. R., van Gorkom, J. H., & Heiles, C. E. 1983, ApJS, 53, 591
Grandi, S. A. 1981, ApJ, 251, 451
Grewing, M., & Mebold, M. 1975, A&A, 42, 119
Hackney, R. L., Hackney, K. R., & Kondo, Y. 1982, in Advances in Ultraviolet Astronomy: Four Years of *IUE* Research (NASA CP-2238), 335
Haschick, A. D., & Burke, B. F. 1975, ApJ, 200, L137
Haxthausen, E., Carilli, C. L., & van Gorkom, J. H. 1990, Contributed paper in Tetons Conference on the Interstellar Medium in External Galaxies, ed. D. Hollenbach & H. A. Thronson (NASA CP-3084), 356
Hubbard, R., Brault, J., Engleman, R., & Palmer, B. 1983, unpublished report, Kitt Peak National Observatory
Hudson R. D., & Carter V. L. 1967, J. Opt. Soc. Am., 57, 651
Osterbrock, D. E. 1989, Astrophysics of Gaseous Nebulae and Active Galactic Nuclei (Mill Valley: Univ. Science Books)
Pesch, P., Westpfahl, D. J., & Simkin, S. M. 1990, PASP, 102, 427
Phillips, A. P., Pettini, M., & Gondhalekar, P. M. 1984, MNRAS, 206, 337
Rand, R. J., Kulkarni, K. R., & Hester, J. J. 1990, ApJ, 352, L1
Reilman, R. F., & Manson, S. T. 1979, ApJS, 40, 815
Routly, P. M., & Spitzer, L. 1952, ApJ, 115, 227
Rubin, V. C., Thonnard, N., & Ford, W. K. 1982, AJ, 87, 477 (RTF)
Sargent, W. L. W., Young, P. J., Boksenberg, A., & Tytler, D. 1980, ApJS, 42, 41
Schneider, S. E. 1985, ApJ, 288, L33
———. 1989, ApJ, 343, 94
Shull, J. M. 1978, ApJ, 226, 858
Shull, J. M., & Van Steenberg, M. E. 1985, ApJ, 294, 599
Shull, J. M., York, D. G., & Hobbs, L. M. 1977, ApJ, 211, L139
Siluk, R. S., & Silk, J. 1974, ApJ, 192, 51
Songaila, A., Bryant, W., & Cowie, L. L. 1989, ApJ, 345, L71
Spitzer, L. 1978, Physical Processes in the Interstellar Medium (New York: Wiley Interscience)
Stone, R. P. S. 1977, ApJ, 218, 741
Urry, C. M., & Reichert, G. 1987, *IUE* Newsletter, 34, 95
Wolfe, A. M. 1979, in Proc. NATO Advanced Study Institute, Active Galactic Nuclei, ed. C. Hazard & S. Mitton (Cambridge: Cambridge Univ. Press), 159
York, D. G., Dopita, M., Green, R., & Bechtold, J. 1986, ApJ, 311, 610